Probing the Defect Structure of Anion-Excess $Ca_{1-x}Y_xF_{2+x}$ (x = 0.03−0.32) with High-Resolution ^{19}F Magic-Angle Spinning Nuclear Magnetic Resonance Spectroscopy

Francis Wang and Clare P. Grey*

Department of Chemistry, State University of New York at Stony Brook, Stony Brook, New York 11794-3400

Received March 26, 1998. Revised Manuscript Received June 18, 1998

Fluorine-19 magic-angle spinning nuclear magnetic resonance spectroscopy (^{19}F MAS NMR) was used to study the local structure and fluoride ion environments in the anion-excess cubic fluorite material $Ca_{1-x}Y_xF_{2+x}$ ($0 < x \leq 0.32$). Four distinct ^{19}F resonances were observed at spinning speeds of >20 kHz; these have been assigned to three different types of sites: two interstitial sites, sites that have relaxed slightly from the normal sites of the fluorite structure, and the normal sites. Very similar spectra were observed for the mineral Tveitite ($x \approx 0.25-0.27$), which contains an ordered calcium yttrium−fluoride phase with excess fluoride ions located in cuboctahedron clusters. Only three resonances were observed for this high-yttrium-content material, which were assigned to the normal, relaxed, and interstitial fluoride ions that make up the cuboctahedron. The similarity between the spectra of the synthesized materials and Tveitite indicate that similar clusters are present. The resonances due to the interstitial sites are assigned to fluoride ions in cuboctahedra or square antiprisms and the additional interstitial ions associated with these clusters. The changes in intensities of these resonances are consistent with the increase in the cuboctahedron: square antiprism ratio at higher doping levels. Variable-temperature NMR shows that the anions within the clusters are mobile and undergo exchange with each other. At higher temperatures and doping levels, exchange involving the relaxed and normal fluoride ions also occurs.

Introduction

Many halides ($M^{2+}X_2^-$) with the fluorite structure can accommodate a large number of excess anions when extrinsically doped with, for example, $D^{3+}X_3^-$ compounds. The D^{3+} dopant cations substitutionally occupy M^{2+} cation sites, and overall charge neutrality is maintained by incorporating excess X^- anions into vacancies within the fluorite structure. The $Ca_{1-x}Y_xF_{2+x}$ anion-excess fluorite system is an extensively studied defect system in which the excess anions are reported to order into defect clusters.[1−3] A number of cluster defect models have been developed to explain the experimental data.

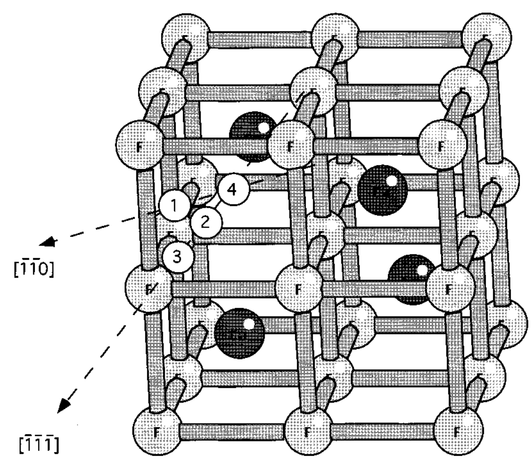

Figure 1. The CaF_2 fluorite structure. The location of the excess and relaxed fluorine sites, F1, F2, F3, and F4, are shown in the foremost top-left octant of the fluorite structure.

The fluorite structure, shown in Figure 1, adopts the $Fm\bar{3}m$ space group, with cations in 4a sites at (0,0,0) and anions in 8c sites at (1/4,1/4,1/4). The structure can be thought of as a cubic array of fluorine anions with

* Author to whom correspondence should be sent. E-mail: clare.grey@sunysb.edu.

(1) Cheetham, A. K.; Fender, B. E. F.; Steele, D.; Taylor, R. I.; Willis, B. T. M. *Solid State Commun.* **1970**, *8*, 171−173.
(2) Cheetham, A. K.; Fender, B. E. F.; Cooper, M. J. *J. Phys. C: Solid State Phys.* **1971**, *4*, 3107−3121.
(3) Laval, J. P.; Mikou, A.; Frit, B. *Solid State Ionics* **1988**, *28−30*, 1300−1304.
(4) Baker, J. M.; Davies, E. R.; Hurrell, J. P. *Proc. R. Soc.* **1968**, *A308*, 403−431.
(5) Moore, D. S.; Wright, J. C. *J. Chem. Phys.* **1981**, *74*, 1626−1635.
(6) Laval, J. P.; Frit, B. *J. Solid State Chem.* **1983**, *49*, 237−246.
(7) Willis, B. T. M. *Proc. Br. Ceram. Soc.* **1964**, *1*, 9−19.
(8) Bevan, D. J. M.; Strahle, J.; Greis, O. *J. Solid State Chem.* **1982**, *44*, 75−81.
(9) Catlow, C. R. A.; Chadwick, A. V.; Greaves, G. N.; Moroney, L. M. *Nature* **1984**, *312*, 601−604.
(10) Catlow, C. R. A.; Chadwick, A. V.; Corish, J.; Moroney, L. M.; O'Reilly, A. N. *Phys. Rev. B* **1989**, *39*, 1897−1907.
(11) Laval, J. P.; Mikou, A.; Frit, B. *J. Solid State Chem.* **1990**, *85*, 133−143.

10.1021/cm980192l CCC: $15.00
Published on Web 09/05/1998

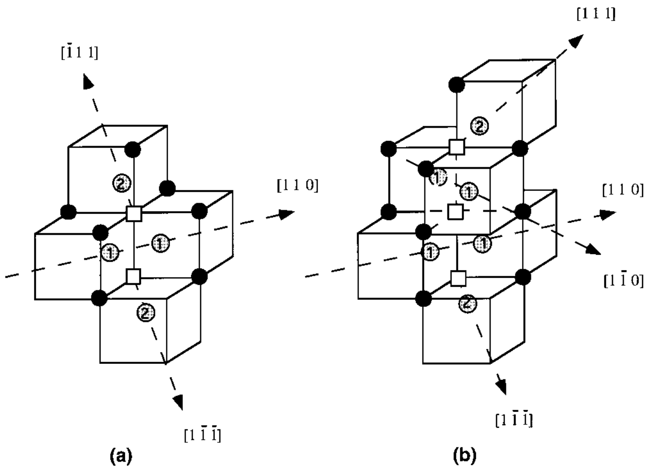

Figure 2. Schematic diagram of (a) the 2:2:2 and (b) the 3:4:2 defect cluster models. Surrounding relaxed F3 sites are represented by dark spheres. For clarity, only 7 out 10 and 9 out of 14 of these F3 sites are shown in a and b, respectively. Open squares represent vacant fluorine sites.

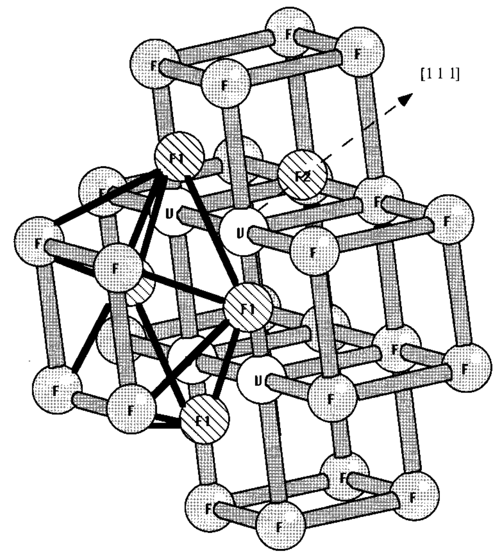

Figure 3. Schematic diagram of the square antiprism defect cluster model with 1 F2 fluorine site. The relaxation of the normal sites (to form F3 sites) is not shown for clarity.

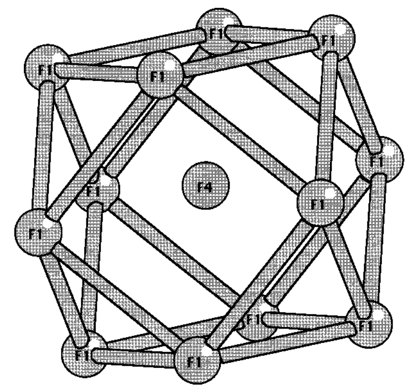

Figure 4. The cuboctahedron defect cluster formed by fusing six square antiprisms. The diagram shows the 12 F1 interstitial sites that make up the cuboctahedron and a central F4 site. Surrounding relaxed F3 and F*n* sites are omitted for clarity.

calcium occupying alternate cube centers. At dilute dopant levels ($x < 0.001$), charge compensation occurs by the formation of dopant−excess anion pairs, where the excess anions occupy the center of the nearest neighbor cubes at (1/2,1/2,1/2), referred to in this study as F4.[4,5] At higher dopant levels ($x > 0.01$), clusters of excess and displaced anions and dopant cations are formed. The earliest defect-cluster models were proposed by Cheetham et al.[1,2] from powder and single-crystal neutron diffraction experiments. The displaced and excess anions were reported to be located on two sites, termed F1 and F2. The F1 and F2 sites were refined on 48*i* positions at (1/2,u,u) with $u = 0.38$ and 32*f* positions at (w,w,w) with $w = 0.40$, respectively. Reexamination of the original data provided evidence for a further disordered site, F3, on a 32*f* position at (v,v,v) with $v = 0.29$.[6] The close proximity of the F3 position to normal fluorine sites, F*n*, suggested that the F3 sites are slight relaxations off the normal site due to nearby F1 and F2 sites. The locations of the F1, F2, F3, and F*n* sites are shown in Figure 1. Two defect clusters, namely the 2:2:2 and 3:4:2 defect clusters, were proposed (Figure 2a,b), and were based on previous cluster models developed for the UO_{2+x} defect system.[1,2,7] The 2:2:2 notation indicates a defect cluster containing two vacancies, two F1 anions, and two F2 anions, with accompanying relaxed F3 anions. One difficulty, however, with the 2:2:2 and 3:4:2 defect cluster models was the presence of very short (<2 Å) F1−F1 distances. This resulted in Laval and Frit[6] developing an alternative defect model in which a single (Ca,Y)F_8 fluorite cube is converted into a square antiprism, as shown in Figure 3. The square antiprism defect model contains four anions on F1 sites, four vacancies on F*n* sites, and between one and four excess anions located along the ⟨111⟩ direction in F2 sites. More recently, the structure refinement and characterization of the ordered calcium−yttro fluorite mineral Tveitite[8] has led to the proposition that the excess anions in $Ca_{1-x}Y_xF_{2+x}$ can form an octahedral arrangement of six square antiprisms sharing corners to enclose a cuboctahedron of anions with an additional anion (F4) in its center (Figure 4).[3,8−12] An additional cuboctahedron model has also been proposed with two extra anions in F2 sites along the ⟨111⟩ direction of the fluorite lattice.[13]

The results of a ^{19}F very fast magic-angle spinning nuclear magnetic resonance (MAS NMR) study of $Ca_{1-x}Y_xF_{2+x}$ ($x = 0.03-0.32$) are presented in this paper. The ^{19}F MAS NMR spectra of $Ca_{1-x}Y_xF_{2+x}$, collected at spinning speeds in excess of 20 kHz, show sufficiently high-resolution spectra to allow multiple resonances from interstitial and relaxed normal sites to be observed and assignments, based upon relative intensities, to be made. The intensities of the observed resonances are compared with those calculated for various defect models. High-temperature ^{19}F MAS NMR spectra of $Ca_{1-x}Y_xF_{2+x}$ ($x = 0.03-0.32$) are used to examine the mobility of individual sites within the defect clusters. The ^{19}F MAS NMR spectra are also collected for the mineral Tveitite and are compared with those of synthesized $Ca_{1-x}Y_xF_{2+x}$ ($x = 0.03-0.32$).

(12) Laval, J. P.; Abaouz, A.; Frit, B. *J. Solid State Chem.* **1989**, *81*, 271−277.
(13) Hull, S.; Wilson, C. C. *J. Solid State Chem.* **1992**, *100*, 101−114.

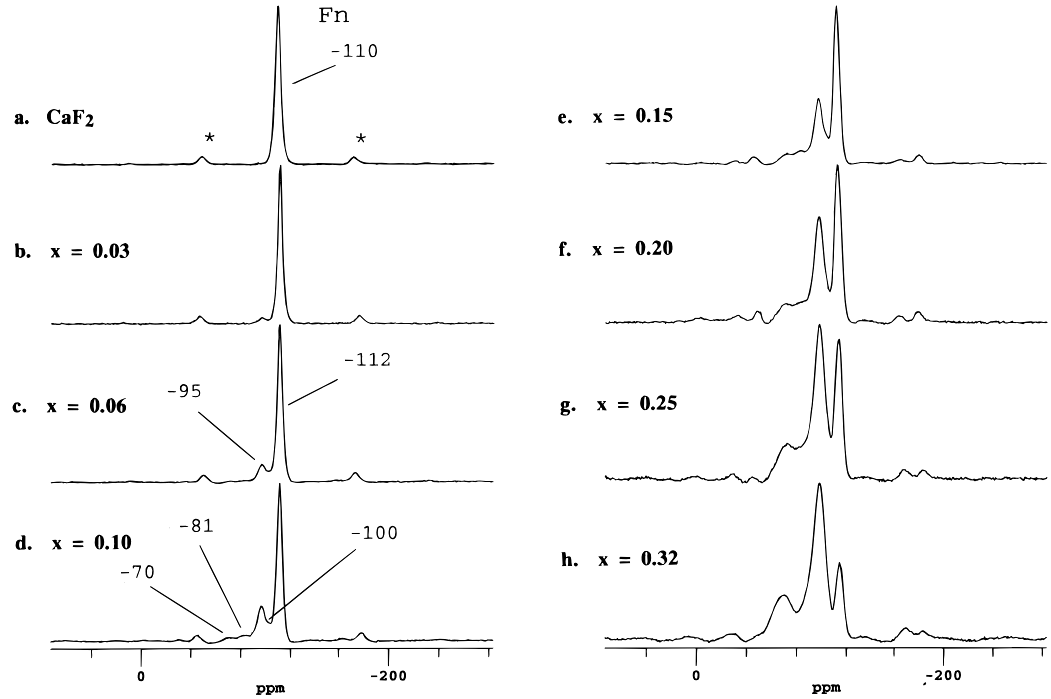

Figure 5. Room-temperature ^{19}F MAS spectra of (a) CaF_2 and (b−h) $Ca_{1-x}Y_xF_{2+x}$ ($x = 0.03-0.32$) collected at spinning speeds of 21−22 kHz: (a) CaF_2; (b) $x = 0.03$; (c) $x = 0.06$; (d) $x = 0.10$; (e) $x = 0.15$; (f) $x = 0.20$; (g) $x = 0.25$; (h) $x = 0.32$. The symbol * denotes spinning sidebands. The isotropic resonances are marked on representative spectra.

Experimental Section

Materials Preparation. Samples of $Ca_{1-x}Y_xF_{2+x}$ ($x = 0.03-0.32$) were synthesized by thoroughly mixing appropriate amounts of CaF_2 (Aldrich 99.9%) and YF_3 (Aldrich 99.9%), pressing the mixed samples into pellets, and firing the samples at 1100 °C for 24 h in evacuated quartz tubes. X-ray powder diffraction patterns of all the samples confirmed the presence of only one phase. The ^{19}F MAS NMR of the samples confirmed that no residual unreacted YF_3 remained. A 1.8-g sample of the mineral Tveitite was obtained from Dr. Gunnar Raade of the Mineralogisk-Geologisk Museum in Oslo, Norway.

NMR Measurements. The ^{19}F MAS NMR measurements were performed on a 360 MHz Chemagnetics spectrometer at an operating frequency for ^{19}F of 338.75 MHz. Use of a double-resonance Chemagnetics pencil probe equipped with 3.2-mm rotors, allowed spinning speeds of up to 24 kHz to be attained. The ^{19}F MAS NMR spectra were referenced to CCl_3F at 0 ppm.

Results

One-Dimensional (1-D) ^{19}F MAS NMR. The room-temperature ^{19}F MAS NMR spectra of $Ca_{1-x}Y_xF_{2+x}$ ($x = 0.03-0.32$), collected at spinning speeds in excess of 20 kHz, are shown in Figure 5a−h. The room-temperature spectra of CaF_2 shows a single resonance at −110 ppm, which is assigned to the 8*c* fluorine site (F*n*) of the fluorite structure. The room-temperature ^{19}F MAS NMR spectra of $Ca_{1-x}Y_xF_{2+x}$ ($x = 0.03-0.32$) show a resonance at −112 ppm, due to the normal fluorine site of the fluorite structure (F*n*), and four additional resonances at −70, −81, −95, and −100 ppm. The resonances at −112, −70, −81, and −95 ppm are well resolved at nearly all doping levels, whereas the resonance at −100 ppm is most clearly observed at a doping level of $x = 0.10$ (Figure 5d) and is also clearly observed in the spectra acquired at higher temperatures (presented later). The relative intensities of the five resonances can be estimated by deconvolution of the spectra and are plotted in Figure 6 as a function of doping level.

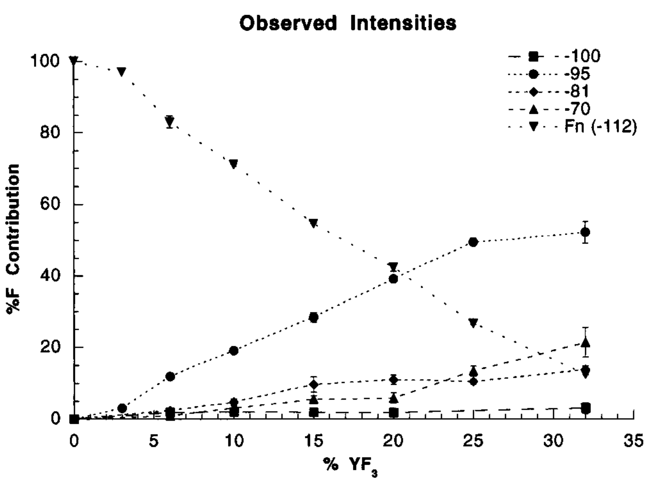

Figure 6. Plot of the change in relative intensities of the five resonances (%) as a function of YF_3 doping level for $Ca_{1-x}Y_xF_{2+x}$ ($x = 0.03-0.32$).

The relative intensity of the resonance at −112 ppm decreases linearly as the YF_3 doping level increases, until at $x = 0.32$, the resonance at −112 ppm represents only 13% of the total amount of fluorine. The second most intense resonance at −95 ppm increases linearly over doping levels of $0.03 \le x \le 0.25$. At doping levels higher than $x = 0.25$, the contribution of the resonance at −95 ppm begins to level off, and by $x = 0.32$, consists of 55% of the total amount of fluorine. The resonance at −81 ppm is slightly more intense than the resonance at −70 ppm at $x = 0.10-0.20$, but at higher concentrations ($x > 0.20$), the intensity of the resonance at −70 ppm is greater. The small intensity of the resonance at −100 ppm along with the overlapping broad resonance at −95 ppm make accurate deconvolution of the resonance at −100 ppm extremely difficult, especially at low and high doping levels. Therefore, the relative concentrations of the resonance at −100 ppm are not reported at doping levels lower than $x = 0.06$ or higher than $x = 0.20$, although the presence of this resonance is evident in the high-temperature spectra of these samples. The deconvolutions of these broad overlapping resonances are difficult, and there is considerable error associated with the intensity measurements, particularly for the low-intensity resonances. The error bars given on the plots represent the range of values that can be used and still achieve reasonable fits to the experimental data. The errors associated with these measurements are still, however, small enough to allow comparison with the different cluster models (vide infra).

The high-temperature ^{19}F MAS NMR spectra of $Ca_{1-x}Y_xF_{2+x}$ ($x = 0.06-0.32$) are shown in Figure 7a−f. Only very small changes are observed in the spectra of the samples with lower doping levels ($x = 0.06-0.10$), as the samples are heated to 250 °C. The resonances at −95 and −112 ppm show small shifts to higher frequency as the temperature is increased, and by 250 °C, the two resonances have shifted between 0.9 and 1.5 ppm, with no significant changes in line width. The resonance at −100 ppm is now clearly resolved. The resonances at −70 and −81 ppm broaden with increasing temperature, particularly at a doping level of $x = 0.10$. The high-temperature spectra of the higher-doping-level samples ($x = 0.15-0.32$) are characteristic of increased fluoride ion mobility.[14] At doping levels $x = 0.15-0.20$, the resonances at −70 and −81 ppm show a gradual increase in line width above 80 °C, and by 250 °C, they appear as a broad shoulder on the resonance at −95 ppm. The line widths of the resonances at −95 and −112 ppm also increase, and at temperatures >200 °C, have increased by ≈100 Hz from their room-temperature values. At higher doping levels (i.e., $x = 0.25-0.32$), the broadening of the resonances at −70 and −81 ppm is followed by coalescence to a single resonance. Coalescence will occur when the fluoride ions giving rise to the resonances at −70 and −81 ppm exchange with a rate greater than their frequency separation (i.e., 3.7 kHz). The line widths of the resonances at −95 and −112 ppm were observed to increase above 150 and 200 °C for $x = 0.25$ and 0.32, respectively, as the fluoride ions associated with these resonances begin to exchange with the mobile fluoride ions. By 250 °C, the resonance due to the mobile ions has shifted to −87 and −83 ppm for $x = 0.25$ and 0.32, respectively, and is no longer intermediate in chemical shift between the resonances at −70 and −81 ppm, as expected for two-site exchange. This shift confirms that fluoride ion exchange at this temperature includes not only fluoride ions from the resonances at −70 and −81 ppm, but also fluoride ions originally resonating at −95 and −112 ppm. Furthermore, the relative intensity of the resonance at −95 ppm decreases with temperature, indicating increased exchange processes (Figures 7e and f). This decrease is accompanied by an increase in the intensity of the resonance assigned to the mobile fluoride ions at ≈−83 ppm. No pronounced decrease in the resonance at −112 ppm is observed indicating that this resonance is associated with less mobile ions. Note that the spinning sidebands from all the resonances decrease in intensity consistent with reduced ^{19}F homonuclear dipolar coupling and increased mobility.

The room-temperature ^{19}F MAS NMR spectrum of the mineral Tveitite [$Ca_{1-x}Y_xF_{2+x}$ ($x = 0.263$)] is shown in Figure 8. The spectrum is dominated by at least three broad resonances at −107, −92, and −71 ppm. There are a number of additional low-intensity resonances that are assigned to fluorine-containing impurities (*I*) that are known to be present in the mineral sample. Elemental analysis of Tveitite in previous studies has shown that the mineral also contains low concentrations of paramagnetic impurities and rare-earth oxide-fluorides.[7,15] These impurities could account for the broader resonances observed in the Tveitite spectrum in comparison with the resonances obtained for the synthesized samples of $Ca_{1-x}Y_xF_{2+x}$. The relative intensities of the three resonances of Tveitite were deconvoluted, giving relative intensities for the resonances at −107, −92, and −71 ppm of 19 ± 2, 52 ± 3, and 31 ± 4, respectively. Again, errors arise from severe overlap and the difficulty of deconvolution of all the overlapping spinning sidebands (and from possible impurity phases).

Discussion

Five different fluorine environments were resolved in the ^{19}F MAS NMR spectra of $Ca_{1-x}Y_xF_{2+x}$ ($x = 0.03-0.32$). Comparisons can now be made between the calculated relative occupancies of the interstitial and displaced fluorine sites of the defect cluster models and the relative intensities of the observed spectra. The calculated concentrations of the different types of fluoride-ion sites are plotted in Figure 9a−j for the 10 defect cluster models, which are variants of the three basic clusters. These clusters were previously used by Wilson et al.[13] to fit site occupancies obtained from diffraction data. These site occupancies were calculated assuming discrete defect clusters, with no sites, including the relaxed normal sites (F3), being shared by two or more clusters. The experimentally determined concentration of the normal site of the fluorite structure F*n* (the resonance at −112 ppm) and the resonance at −95 ppm are plotted for comparison.

The calculated fluorine occupancies of the 1−3 ⟨110⟩ F1 pair defect cluster models are shown in Figures 9a−c and involve between one and three sets of F1 pairs clustered together to accommodate excess fluorine ions. The 1 and 2 ⟨110⟩ F1 pair clusters correspond to the 2:2:2 and 3:4:2 clusters shown in Figures 2a and b, respectively. The 1 ⟨110⟩ F1 pair model incorporates fewer excess anions per defect cluster than either the 2 or 3 ⟨110⟩ F1 pair defect model, and therefore, the 1 ⟨110⟩ F1 pair model requires more clusters per doping level to accommodate excess anions, resulting in more F3 relaxed fluoride ions than for the other two clusters. The calculated fluorine occupancies for the square antiprism +1−4 F2 ions cluster models are shown in Figures 9d−g (see Figure 3). Increasing the number of F2 fluorine anions per cluster (i.e., the number of excess anions accommodated by each square antiprism) results

(14) For examples, Wang, F.; Grey, C. P. *J. Am. Chem. Soc.* **1998**, *120*, 970−980; *Chem. Mater.* **1997**, *9*, 1068−1070.

(15) Bergstol, S.; Jenson, B. B.; Neumann, H. *Lithos* **1977**, *10*, 81−87.

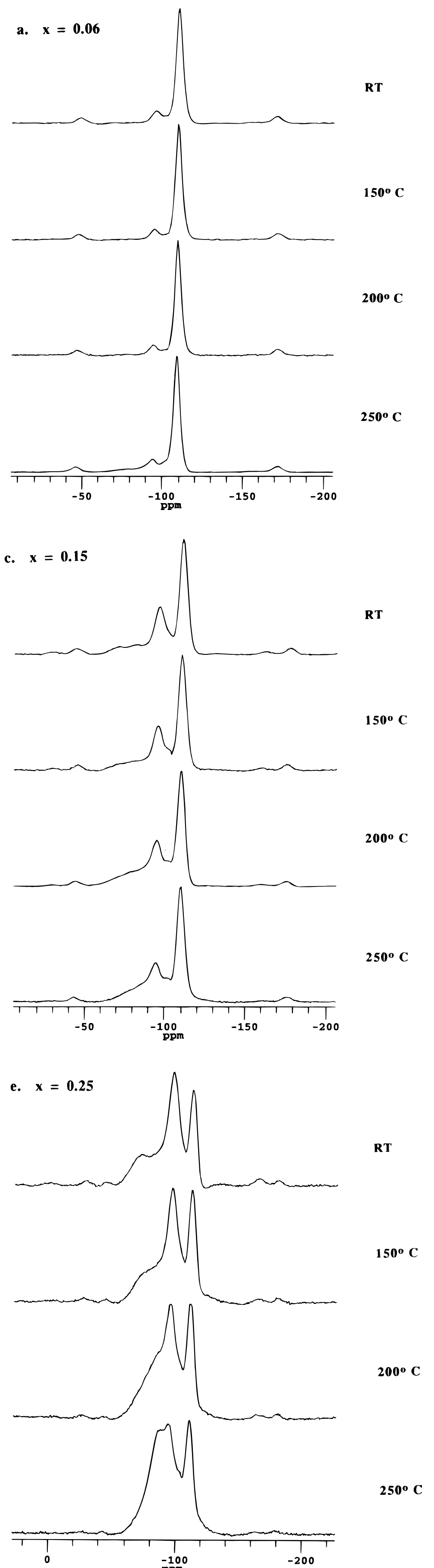

Figure 7. Variable-temperature ^{19}F MAS spectra of $Ca_{1-x}Y_xF_{2+x}$ ($x = 0.03-0.32$) collected at spinning speeds of 21−22 kHz: (a) $x = 0.06$; (b) $x = 0.10$; (c) $x = 0.15$; (d) $x = 0.20$; (e) $x = 0.25$; (f) $x = 0.32$.

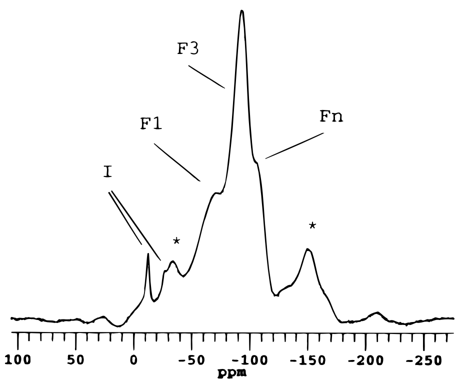

Figure 8. Room-temperature ^{19}F MAS spectra of Tveitite ($Ca_{1-x}Y_xF_{2+x}$ (x = 0.263)) collected at 20 kHz. Fluorine sites F1(−71 ppm), F3(−92 ppm), and F*n*(−107 ppm) are labeled. The symbol * and *I* denote spinning sidebands and impurity phases, respectively.

in a decrease in the relative number of clusters and, hence, the number of F1 fluorine sites required to accommodate excess anions. Thus, the number of discreet square antiprism clusters that can be accommodated by the square antiprism +1 F2 and +2 F2 models, without two clusters sharing the same F3 relaxed fluorine sites, reaches a maximum at x = 18.6 and 28.4, respectively. The calculated occupancies for the cuboctahedron defect models are shown in Figures 9h−j. The cuboctahedron defect structure (shown in Figure 4) incorporates four excess anions per defect cluster. Variations of the cuboctahedron model, involving additional excess anions in the form of a central F4 site or ⟨111⟩ F2 interstitials, provide even more efficient incorporation of excess anions. The number of discreet cuboctahedron and cuboctahedron +1 F4 ion clusters that can be accommodated by these models reaches a maximum at x = 25.2 and 30.8, respectively. Above these values, no more normal fluorine sites remain, and additional excess anions can only be accommodated by defect clusters sharing relaxed F3 fluorine sites.

The number of resonances (four) in the observed spectra, due to interstitial and relaxed sites, is more than any one model predicts. This result suggests that the synthesized $Ca_{1-x}Y_xF_{2+x}$ (x = 0.03−0.32) contains either more than one type of cluster or that the clusters are more disordered or distorted than these models predict. Comparison between the observed relative intensities for the F*n* (−112 ppm) fluorine site with the calculated values for the different defect cluster models allows a number of models to be ruled out. The defect cluster models involving 2 and 3 ⟨110⟩ F1 pairs (Figures 9b and c) have different predicted decreases in F*n* relative intensities, significant deviations being observed at higher dopant levels where increased concentrations of these clusters might be expected. These models are, therefore, extremely unlikely to be present in large concentrations. Similarly, square antiprisms with only 1 or 2 F2 interstitials (Figures 9d and e) and cuboctahedrons without either additional interstitials (F4 or F2 ions) do not appear to be present in sizable concentrations. Furthermore, the almost linear decrease in F*n* intensity suggests that if more than one type of cluster is present, then the ratios of the concentrations of the different clusters must remain fixed with doping level or the F*n* concentrations must be similar for the different clusters. Based only on the F*n* intensity, we are able to exclude five out of the 10 different models.

The relaxed F3 sites will have the highest relative intensity of the interstitial or relaxed fluorine sites in all defect models. The resonance at −95 ppm is, therefore, assigned to this site, because this site has the highest relative intensity of the four resonances from interstitial or relaxed sites (−70, −81, −95, and −100 ppm). The plot of the experimentally observed percent F3 concentration versus doping level has also been plotted with the calculated F3 intensities in Figure 9, and shows a linear increase with increasing doping level up to x = 0.25. As for the F*n* site, defect clusters that are present in significant concentrations should have similar increases in fluorine contribution as a function of doping level, particularly at doping levels $x < 0.20$, where cluster overlap should be less significant. The F3 concentrations for the ⟨110⟩ F1 pairs, square antiprisms + 2−4 F2, cuboctahedron + F4, and cuboctahedron + ⟨111⟩ F2 cluster models all show reasonable fits to the experimental data. Again, the cuboctahedron, and square antiprism +1 F2 defect cluster models can be excluded as major cluster types. The square antiprism with 2 F2s and the 2 and 3 ⟨110⟩ F1 pairs clusters cannot be totally excluded on the basis of F3 intensities.

Of the remaining possible defect cluster models, there are three other possible fluorine sites that could be assigned to the remaining unassigned resonances (−71, −81, and −100 ppm), namely F1, F2, and F4. The resonance due to the F4 fluorine site in the cuboctahedron + F4 defect cluster model is predicted to have an extremely low concentration for all the calculated doping levels, even if this is the only cluster present; hence, this site cannot be assigned to either the resonance at −71 and −81 ppm. These two resonances are, therefore, assigned to the F1 and F2 sites. Furthermore, these two resonances coallesce at higher intensities, strongly suggesting that they are part of the same cluster. The intensities of the three resonances are plotted versus the calculated intensities of the F1, F2, and F4 sites for the five cluster models that gave reasonable fits to the experimentally determined F3 and F*n* intensities in Figures 10a−e. No model provides a perfect fit to the experimentally observed intensities at all loading levels. The intensities of the resonances at −70 and −81 ppm are nearly equal for doping levels of up to x = 0.25, suggesting that these arise from the models containing F1 and F2 interstitials in equal ratios. The agreement between calculated and predicted intensities is reasonable, given the strong overlap of these resonances, for the 2:2:2 cluster and the square antiprism with 3 or 4 F2 ions (Figures 10a−c). It is impossible to distinguish between the 2:2:2 cluster and the square antiprism with 4 F2 ions on the basis of intensity calculations only. Furthermore, the accuracy of our spectral deconvolutions is not sufficient to distinguish between square antiprisms with 3 or 4 F2 clusters. However, the model with fewer F2 ions provides a better fit at higher doping levels, which appears unlikely. The cuboctahedron model does not provide a very good fit to the data unless both the resonances at −70 and −81 ppm are assigned to F1 ions in a distorted cuboctahedron cluster.

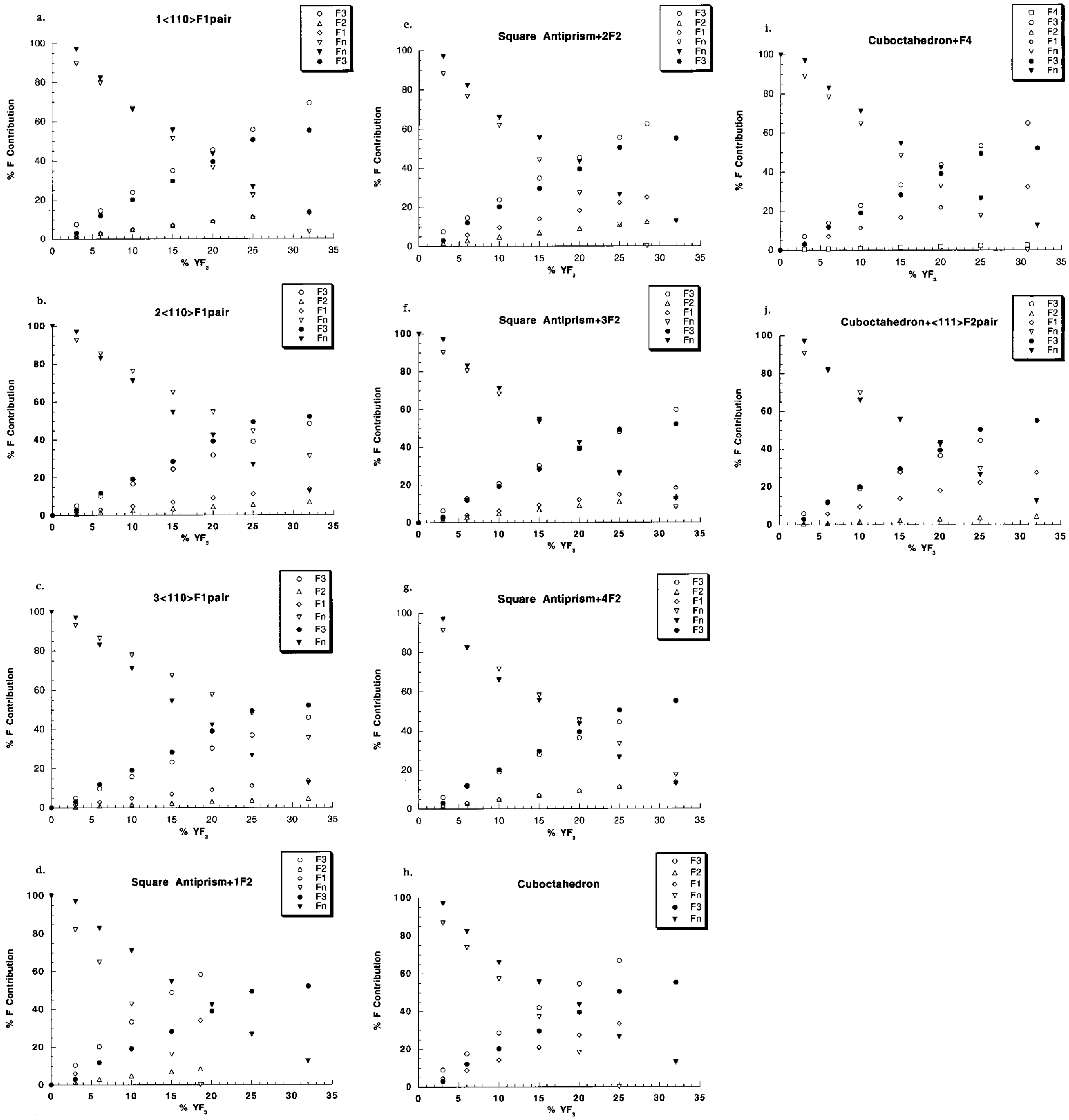

Figure 9. Plots of the site occupancies (%) for the different fluorine sites (F1, F2, F3, F4, F*n*) as a function of YF_3 doping level for various defect cluster models (open data points): (a−c) 1−3 ⟨110⟩ F1 pairs; (d−g) square antiprism with 1−4 F2 fluorine sites; (h) cuboctahedron; (i) cuboctahedron + central F4 ion; (j) cuboctahedron + 2 ⟨111⟩ F2 ions. The experimentally observed relative intensities of the resonances assigned to F3 (−95 ppm) and F*n* (−112 ppm) sites are also shown as filled data points for comparison.

Additional insight into the nature of the clusters can be obtained from the spectrum of Tveitite. Previous diffraction studies of Tveitite have shown that the structure consists of discrete M_6X_{37} cuboctahedron clusters (with central F4 atom) distributed in a fluorite lattice.[8] The refinement of the structure of Tveitite, in space group $R\bar{3}$, yields eight different fluorine sites.[8] There are two interstitial fluorine sites (closely related to F1 in this study) that make up the cuboctahedron and account for 28% of the fluoride ions, four relaxed sites (F3 in this study; 56% of the fluoride ions), and a single interstitial site at the center of the cuboctahedron (F4 in this study; 2.3%). The final site, which accounts for 14% of the fluoride content, is closest to a normal site and is adjacent to calcium cations only (unlike the other sites). The local environment of this site differs slightly from a normal fluorite site, containing F1 and F3 sites in its local coordination sphere of fluorine ions. Sites with similar environments were, however, classified as F*n* in the other models because they are located on the (1/4, 1/4, 1/4) site of the fluorite structure. Unfortunately, Tveitite is not monophasic and consists of the ordered rhombohedral phase and a disordered cubic solid solution. An overall chemical composition

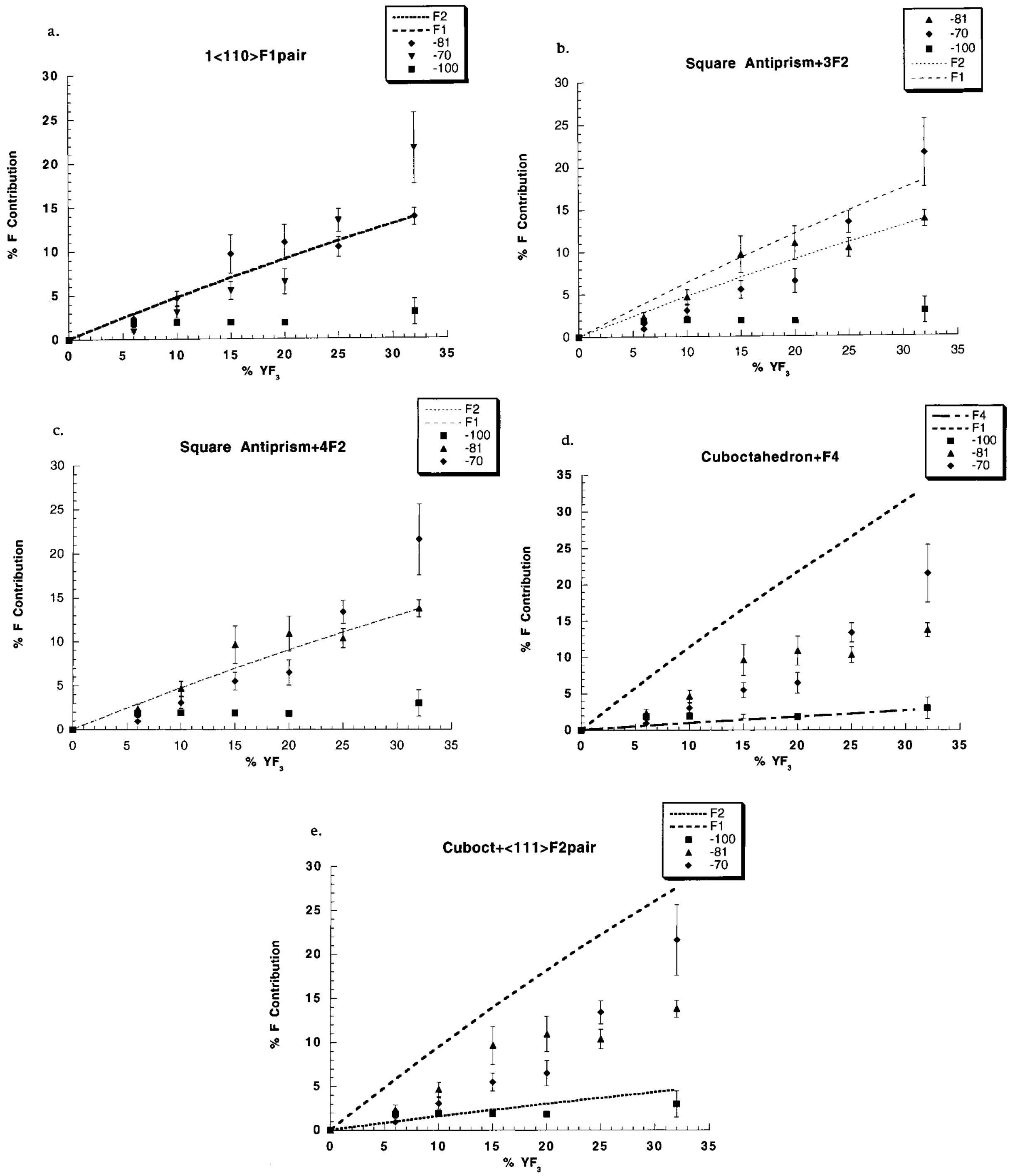

Figure 10. The calculated site occupancies for various defect cluster models, and of the observed relative intensities of the resonances at −100, −81, and −70 ppm, are plotted versus doping level, for the following defect cluster models: (a) 1 ⟨110⟩ F1 pair; (b) square antiprism + 3 F2 ions; (c) square antiprism + 4 F2 ions; (d) cuboctahedron + F4 ions; (e) cuboctahedron + 2 ⟨111⟩ F2 ions.

of $MX_{2.252}$ with a Ca:(Y + Ln) ratio of 2.24[15] was determined previously. The rare earth ion impurities and oxygen were thought to be present as oxyfluorides, although the possibility that the oxygen is located in the center of the cuboctahedron, as was assumed in the compound $Nd_{14}Cl_{32}O$,[16] was discussed. The sharper impurity resonances observed experimentally are consistent with the former suggestion and appear to result from the presence of fluoride ions in solids containing lower concentrations of fluoride ions such as oxyfluorides: fluoride ions in these environments will be less strongly dipolar-coupled and thus the homonuclear coupling will be more readily removed by MAS, leading to narrower resonances. By assuming the presence of oxyfluorides, a formula for the calcium yttrium fluoride phases of $Ca_{13.89}Y_{5.07}F_{43}$ was calculated previously.[8] In contrast, the Tveitite refinement yields a composition of $Ca_{13}Y_6F_{43}$.[8] To reconcile these two numbers, it was proposed that sites ascribed to ytrrium in the refinement may in fact be partially occupied by calcium.

(16) Lochner, U. Ph.D. Thesis, Karlsruhe, 1980.

Three major broad resonances were observed in the ^{19}F MAS NMR spectra of Tveitite. The increased broadening of these resonances in comparison with the synthesized materials is either due to paramagnetic impurities within the sample or to a greater distribution in local environments for the fluoride ions in the sample. The resonances at −92 and −107 ppm are assigned to F3 relaxed fluoride ions and F*n* fluorine sites, respectively, based on the chemical shift of CaF_2 (−110 ppm), and by comparing the relative intensities of the resonances with those predicted from the structure of the mineral. The remaining resonance at −71 ppm is, therefore, assigned to the interstitial F1 site of the cuboctahedron. The experimental F1:F3:F*n* ratio of 19 ± 2:52 ± 3:31 ± 4 differs from that predicted from the structure of the ordered rhombohedral phase 28:56:14 (ignoring the small contribution from the F4 site, 2.3%, that was not observed experimentally). The much higher F*n* intensity suggests that the additional cubic phase that is also known to be present in Tveitite[8] contains a lower concentration of YF_3. This result may help explain the discrepancy between the yttrium content of the ordered phase and the overall yttrium content of Tveitite. The Tveitite spectrum provides strong confirmation that the assignment of the resonance at −95 ppm from the synthesized materials to the F3 sites is correct, and suggests that the resonance at −71 ppm arises from ions in a cuboctahedron or the very similar square antiprism local environment. Small differences in chemical shift (1−5 ppm) beween the resonances of the synthesized samples and those for Tveitite may be due to small differences in local environment due to the different space group, local distortions of the clusters, or differences in Ca/Y ordering in the clusters.

The F1 local environment in the 2:2:2 cluster, with its very short F1−F1 contact, is very different from the F1 local environment in the square antiprism or cuboctahedron, where there are no unusually short distances.[2] It therefore appears extremely unlikely that the resonance at −70 ppm in the spectra of the synthesized materials arises from F1 ions in the 2:2:2 cluster, and we assign the resonance at −70 ppm to F1 ions in square antiprisms (or cuboctahedra at high doping levels; vide infra). The 2:2:2 cluster type is excluded on this basis. The resonance at −81 ppm is tentatively assigned to the F2 environment. The cuboctahedron was ruled out previously, at low to moderate doping levels, due to the poor fit between the F1 observed and calculated concentrations. Square antiprism clusters with F2 interstitials, therefore, appear to predominate at low-to-moderate loadings. It is not clear whether the slightly higher intensity of the −81 ppm resonance at low-to-intermediate doping levels is real, and efforts are currently underway to acquire spectra at higher fields and with even faster spinning speeds to improve the resolution of the resonances and reduce the errors associated with the spectral deconvolutions. At higher doping levels ($x \geq 0.25$), however, the intensity of the resonance assigned to the F1 ions is significantly more intense than the resonance assigned to F2. This result is ascribed to an increase in the concentration of cuboctahedron clusters, as more and more interstitial anions are accommodated by the fluorite lattice and an increase in ordering and cluster size occurs. An estimate of the square antiprism:cuboctahedron ratio at the highest doping level ($x = 0.32$), obtained from the difference in F1 and F2 intensities, is ∼2:1. The lower than predicted contribution from F3 fluorine sites at high doping levels is attributed to overlap of cuboctahedron and/or square antiprism clusters, resulting in shared F3 relaxed sites. A minimum of five yttrium cations are required per cuboctahedron with a central F4 ion (because this cluster accommodates an additional five fluoride ions). In the structure of Tveitite, these ions were located inside a monocapped square antiprism formed from F1 and F3 ions, the F4 ion forming the cap. Six yttrium ions were located per cluster, although the possibility of partial occupancy by calcium on this site was discussed. The increase in cuboctahedrons formed at higher doping levels is consistent with the large number of yttrium ions needed to form the cluster.

A less satisfactory assignment, where the assignments of the −70 and −81 ppm resonances are reversed is now considered: The resonance at −81 ppm, at low doping levels, is assigned to an F1 resonance in a square antiprism whereas the resonance at ∼−70 ppm is assigned to an F2 resonance in a square antiprism. As the doping level is increased, the resonance at −81 ppm must either shift gradually toward the resonance at −70 ppm, resulting in an apparant increase in the intensity of the −70 ppm resonance, or more likely, the cuboctahedron F1 sites with a slightly different local environment, that are proposed to be present in higher concentrations at higher doping levels, may also resonate at −70 ppm. This assignment is less plausible based on chemical shift arguments outlined in the following paragraph. However, the higher occupancy of the F1 site in comparison with the F2 site that was obtained from the earlier neutron diffraction studies of Cheetham et al.[2] is consistent with this alternative assignment. Other models, based solely on the presence of cuboctahedra may also be considered: To fit the experimental data, a more distorted cuboctahedron with two very different F1 sites (that could then be assigned to the resonances at −70 and −81 ppm) is required at low doping levels. Although two crystallographically distinct F1 sites were refined in the Tveitite structure, these were both required to define the squares of the cuboctahedra because the lower (rhombohedral) space group of this structure does not contain a 4-fold symmetry axis. The two sites could not, however, be separately resolved in Tveitite, suggesting that their environments are very similar. Only one F1 site is required due to the symmetry of the cubic $Ca_{1-x}Y_xF_{2+2x}$ phase and it appears unlikely that local distortions would result in two very disimilar F1 environments in the cuboctahedron, allowing us to rule out this model.

The chemical shifts of the resonances at −95, −81, and −70 ppm will be controlled by the fluoride ion local environments and the deviations of these environments from that of F*n*. The F3 fluorine site ((v,v,v) where v = 0.27)) is a slight relaxation of the F*n* fluorine site (1/4,1/4,1/4) and has a similar local environment to the F*n* fluorine site. The assignment of the F3 relaxed site to the resonance at −95 ppm is reasonable because it is closest in chemical shift (ignoring the small resonance at −100 ppm) to the F*n* site (F3 = −95 ppm and F*n* =

−112 ppm). In contrast, the interstitial fluorine sites, F1 and F2, which have very different local environments than either the F*n* or F3 fluorine sites, have been assigned to the two resonances that are furthest away in chemical shift from the F*n* resonance. The F2 site is also located along the ⟨111⟩ direction and has been refined at (w,w,w) where $w = 0.40$. Finally, the F1 site is located on the 48*i* position at $(1/2,u,u)$ with $u = 0.38$. Because the F2 site is closer to the F3 site than the F1 site, its chemical shift position might be expected to be closer to that of F3, and the assignment of this site to the −81 ppm resonance is consistent with this proposal. The presence of the yttrium cations, inside the square antiprisms, will also affect the chemical shift. ^{19}F MAS NMR of YF_3 was obtained as part of this study, and resonances were observed at −51, −58, and −70 ppm. The shifts observed for the relaxed and interstitial sites of $Ca_{1-x}Y_xF_{2+2x}$ are, therefore, intermediate between those of YF_3 and CaF_2. Furthermore, the F1 ions are coordinated to two yttrium cations, whereas the F3 cations are only coordinated to one, which is consistent with the assignment of the F1 site to the lower frequency resonance.

The resonance at −100 ppm still remains to be assigned. The central F4 site in the cuboctahedron is predicted to have an extremely low concentration for all the calculated doping levels, even if the cuboctahedron is the only cluster present. The resonance at −100 ppm has the smallest relative contribution, and we tentatively assign this resonance to the F4 fluorine site in the cuboctahedron. The intensity of this resonance is extremely difficult to determine, which may account for the discrepancy between predicted and observed intensity. We cannot, however, rule out the possibility that this resonance arises from yet another cluster type in the solid. Two-dimensional spin-diffusion experiments are currently underway to detemine whether the fluoride ions giving rise to this resonance are in close proximity to the fluoride ions giving rise to the resonances at −71 and −80 ppm (i.e., whether they are in the same cluster).

The variable-temperature MAS NMR studies demonstrate that the fluoride ions within the clusters are mobile at higher temperatures. Furthermore, the exchange between different sites suggests the presence of localized clusters of vacancies and interstitials. The onset of mobility occurs among F1 and F2 fluorine sites, as seen by the coalescence of the F1 and F2 sites, becoming more rapid with increasing doping level. At high doping levels ($x = 0.25-0.32$) and high temperatures, the exchanging F1 and F2 fluoride ions begin to exchange with the F3 sites, resulting in a shift of the resonance due to the mobile ions in the direction of the F3 resonance. Some F*n* sites become involved in the motion at even higher temperatures. The onset of mobility in the F1 and F2 fluorine sites suggests that the F1 and F2 sites are in close proximity to each other and to vacancy defects, which is true of all the cluster models presented. The increase in mobility of the F1 and F2 sites at high doping levels is attributed to the closer proximity of the defect clusters, allowing for longer range migration of excess anions through the defect clusters. Some overlap of the defect clusters, or sharing of the relaxed F3 ions, is also evident in the leveling off of the number of F3 relaxed fluorine sites at high doping levels ($x > 0.20$). It has been suggested that the formation of the regular cuboctahedrons may be associated with a decrease in conductivity in comparison with the conductivity associated with the more disordered and open square antiprisms, which is due to the capture of the interstitial ions inside the cuboctahedron.[17] The lower mobility of the ions associated with the resonance at −100 ppm, assigned to F4 ions, is consistent with this suggestion. However, the decrease in F1 mobility that may also be expected is not observed.

Ionic conductivity studies by Reau et al. have shown large increases in the ionic conductivity of $Ca_{1-x}Y_xF_{2+x}$ with increased doping level for $x = 0.05-0.23$.[18] The conductivity did not alter significantly for $x > 0.23$. The increases at intermediate doping levels were interpreted in terms of changes in the extent of clustering, the 2:2:2 defect clusters being progressively replaced 3:4:2 defect clusters at higher dopant concentrations. Because the 3:4:2 cluster is associated with an unbound vacancy, the increase in concentration of the vacancies was proposed to be responsible for the increase in conductivity. No evidence for the presence of the 3:4:2 cluster in any significant concentration was observed in this work. The 2:2:2 cluster was also excluded based on the Tveitite spectra. Our research has demonstrated that the F1 and F2 ions within the clusters are themselves mobile. Long-range conductivity presumably then results from fluoride ion migration between these clusters. Conductivity should then increase with dopant level, as the proximity of the clusters to each other increases, and the activation energy for fluoride-ion migration between clusters decreases. Leveling off in the bulk conductivity is expected at higher loading levels, when all the clusters are connected to or nearby other clusters. Our variable-temperature MAS NMR results demonstrate, however, that the fluoride ion mobility increases with dopant concentration, at least at a short-range, local level, even up to $x = 0.32$.

Conclusions

The normal, interstitial, and relaxed fluoride ion sites of $Ca_{1-x}Y_xF_{2+x}$ ($x = 0.03-0.32$) and the mineral Tveitite were separately resolved for the first time by using very-fast ^{19}F MAS NMR. Comparison of the intensities of these resonances allows a number of cluster models to be ruled out. The similarity of the ^{19}F MAS NMR spectra of the synthesized and Tveitite samples suggests that clusters based on square antiprisms and cuboctahedra are present, rather than the original F1 pair clusters proposed for these systems. The changes in intensity of the resonances assigned to the two types of interstitials, one that is part of the square antiprism and one that is due to additional interstitials (F1 and F2, respectively), suggest that there is as an increase in the concentration of cuboctahedrons over square antiprisms as the doping level is increased. A number of other models were also considered, but these provided less satisfactory fits to the experimentally observed

(17) Reau, J. M.; Matar, S.; Villeneuve, G.; Soubeyroux, J. L. *Solid State Ionics* **1983**, *9–10*, 563–570.
(18) Reau, J. M.; Lucat, C.; Campet, G.; Portier, J.; Hammou, A. *J. Solid State Chem.* **1976**, *17*, 123–129.

intensities of the ^{19}F resonances, and to the expected chemical shifts. Two-dimensional spin diffusion and double-resonance experiments are now in progress to help confirm our assignments and obtain further details concerning the local structure and cation distributions in these clusters. The variable-temperature ^{19}F MAS NMR data demonstrated that although $Ca_{1-x}Y_xF_{2+x}$ is only considered a moderate-to-low fluoride anion conductor at ambient temperatures, there is considerable mobility within the fluoride ion clusters. Exchange with the relaxed and some of the normal sites occurs at higher temperatures and doping levels.

Finally, this work has demonstrated that it is relatively straightforward to observe the interstitial sites in these classes of materials directly. It should, therefore, be possible to investigate the nature of the clusters in a wide range of other fluoride-ion-excess materials by comparing the NMR spectra of known ordered compounds with those of the disordered materials. In addition, it should be possible to determine which of the interstitial sites and/or regular sites in the lattice contribute to the anionic conductivity of the material. Extensions of this work to other systems are currently in progress.

Acknowledgment. Support from the National Science Foundation, for the purchase of a solid-state NMR spectrometer (CHE-9405436), and from the National Young Investigator Program (DMR 9458017) is gratefully acknowledged. We are indebted to Dr. Gunnar Raade of the Mineralogisk-Geologisk Museum (Oslo) for donating the sample of Tveitite to us.

CM980192L